Combinatorial Search for Iron/Titanium-Based Ternary Oxides with a Visible-Light Response

Hitoshi Kusama,* Nini Wang, Yugo Miseki, and Kazuhiro Sayama

Energy Technology Research Institute, National Institute of Advanced Industrial Science and Technology (AIST), AIST Tsukuba Central 5, 1-1-1 Higashi, Tsukuba, Ibaraki 305-8565, Japan

Received December 14, 2009

A combinatorial approach has been carried out to systematically investigate visible-light responsiveness of Fe−Ti−M (M: various metal elements) oxides for photoelectrochemical water splitting. Among the 25 elements tested, strontium was the most effective. A ternary metal oxide with the composition $Fe_{86.1}Ti_{9.6}Sr_{4.3}O_x$ has been identified as a new lead structure for a visible-light responsive, n-type semiconductor. We have conducted various kinds of characterization of the Fe−Ti−Sr oxide semiconductor and discussed the reason why Sr in the Fe−Ti oxide gave the highest photocurrent.

Introduction

Ever since Fujishima and Honda first found that a TiO_2 photoelectrode splits water into oxygen and hydrogen under UV-light irradiation,[1] photoelectrodes and photocatalysts have been important for energy production and environmental purification using solar light. Currently, TiO_2 under UV light is used as a photocatalyst for environmental cleanup.[2] Although great efforts have been made in developing visible-light responsive semiconductors for photocatalysis,[3–12] no efficient ones have been discovered for visible light. In the field of photoelectrodes, nanocrystalline semiconductor thin films with porous structures such as WO_3, Fe_2O_3, and $BiVO_4$ on conducting glass electrodes have shown very high incident photon-to-current conversion efficiencies (IPCE) for water decomposition under visible light,[13–18] compared with single-crystal or pellet-type ones. However, their solar energy conversion efficiencies have been insufficient for practical use with respect to light absorption, energy levels of valence and conduction bands, charge separation, photocurrent−potential dependence, and stability.

In order to utilize sunlight effectively, new semiconductors which would work under visible light with high conversion efficiencies, both as photoelectrodes and photocatalysts, must be discovered and developed. It is challenging to proceed with the search for new semiconductor materials consisting of more than two elements with varying compositions because of the large phase space available. To accelerate the screening of semiconductor materials, their synthesis and evaluation should be automated.

Guided by the above factors, we have developed a high-throughput screening system for new visible-light responsive semiconductors for photoelectrodes and photocatalysts. A photoelectrochemical measurement was selected to evaluate the charge separation capacity of the visible-light responsive semiconductors. In addition, an automated synthesis system for a photoelectrode library (array of samples) using the metal organic decomposition (MOD) method and an evaluation system for screening were developed. Our MOD method uses organic solvents as well as additives (viscosity improver), and the precursor solutions are mixed using an automated liquid-handling platform before printing and firing. This method is best suited to the preparation of mixed oxides and the doping because metal ions are dispersed at the atomic level and stabilized by organic compounds before thermal decomposition by calcination. Furthermore, because of the small amount of samples required, our method is low-cost and environmentally friendly. As a result, in the screening for p-type semiconductors in bismuth-based binary oxides, a new material with high visible-light responsiveness, $CuBi_2O_4$, was discovered.[19] Moreover, during the screening of iron-based binary oxides for n-type semiconductors, we have found several promising new materials quickly and easily, such as Fe(85%)−Ti(15%), Fe(65%)−Zr(35%), and Fe(50%)−V(50%).[20]

In this work, we apply this search method to discover new n-type, ternary-oxide semiconductors consisting of Fe, Ti, and M. We also characterize these new semiconductors in order to elucidate the reason for the high visible-light response.

Experimental Section

Our automated semiconductor synthesis system has been reported previously.[19,20] Fluorine-doped tin oxide (FTO) conductive glass obtained from Asahi Glass Co. was used as the substrate. We used enhanced metal-organic decomposition solutions of various metals purchased from Symetrix Corporation, diluted with *n*-butyl acetate to 0.2 $mol \cdot dm^{-3}$ as precursors. The precursor solutions were mixed in a deep well at the required ratio, and a viscosity improver, prepared by dissolving ethyl cellulose in *n*-butyl acetate at 10 wt %, was added to control the printing conditions. The solutions were printed on a conducting glass substrate using a disposable tip. This system can synthesize 42 samples on the same conductive glass substrate at a time. The printed samples were transferred

* To whom correspondence should be addressed. E-mail: h.kusama@aist.go.jp.

10.1021/cc9001845
Published on Web 03/12/2010

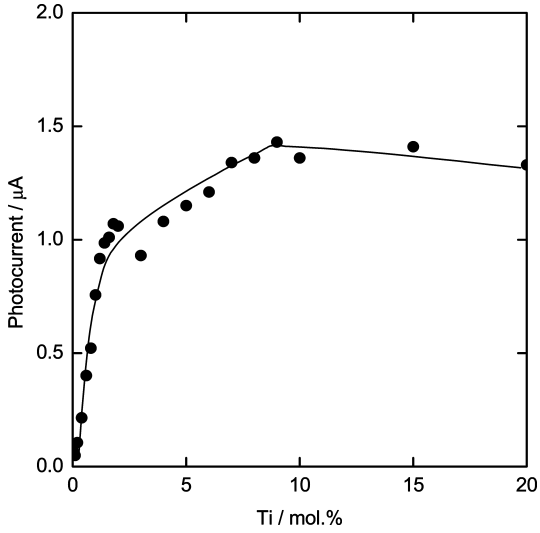

Figure 1. Dependence of the photocurrent on the Ti ratio in Fe−Ti binary oxide photoelectrodes.

into a furnace and fired first at 823 K for 0.5 h and then at 973 K for 0.5 h in air. These printing and firing processes were repeated four times. Some samples were also prepared by spin coating and calcination for various characterizations.

The photocurrents of the synthesized samples were evaluated by scanning the photoelectrode with focused light while applying a constant potential. The photocurrent was measured using a potentiostat (Toho Giken, PS-08) and a Pyrex glass cell. As electrolyte, we used 0.1 mol·dm^{-3} NaH_2PO_4 aqueous solution adjusted to pH 7.0 with NaOH. Cu foil was taped on the top of the photoelectrode to connect the cables to the working electrode. An Ag/AgCl electrode and a Pt wire were used as the reference and counter electrodes, respectively. A Xe lamp (PerkinElmer, CERMAX 300 W) equipped with an optical fiber was used as the light source. A 420 nm cutoff filter (HOYA, L-42) was used for visible-light irradiation. The edge of the optical fiber was covered with a 1 mm diameter slit and fixed on the XY stage to scan the light over the sample. The photocurrent was evaluated by measuring the difference between the current when the light was on (3.2 mW) and the current when the light was off under a constant potential. The potential was set to 1.0 V. The error in the photocurrent measurement was within 6%.

The morphology of the film was observed using a scanning electron microscope (SEM, Hitachi, S-800). Material identification was performed using an X-ray powder diffractometer (XRD, Bruker AXS, MX-Labo) with Cu Kα_1 radiation. Patterns were assigned according to the JCPDS database. Raman spectroscopy was undertaken using a Jasco NRS-1000 Raman spectrophotometer at 532 nm. UV−vis spectra were taken with a Jasco V-570 spectrometer equipped with an integrating sphere, and light-harvesting efficiency (LHE) of the electrode was calculated from its transmittance (T) and reflectance (R):

$$\mathrm{LHE} = 1 - T - R \quad (1)$$

Results and Discussion

Fe−Ti Binary Oxides. As previously reported,[19,20] the photocurrent in the Fe−Ti system showed marked improvement between 5 and 20 mol % Ti concentrations compared to pure Fe oxide. On the basis of this result, we began by investigating the effect of Ti within 20 mol % in detail. As shown in Figure 1, the photocurrent increased with the addition of Ti and reached a maximum at 9 mol %. This behavior was reproducible. We have, thus, fixed the Fe−Ti ratio at 98:2 and at 90:10 for the ternary oxide search.

Table 1. Composition of Samples for the New Visible-Light Responsive Ternary Oxide Search

Fe−Ti ratio = 98:2			Fe−Ti ratio = 90:10		
Fe	Ti	M	Fe	Ti	M
98.0	2.0	0.0	90.0	10.0	0.0
97.9	2.0	0.1	89.9	10.0	0.1
97.8	2.0	0.2	89.8	10.0	0.2
97.7	2.0	0.3	89.7	10.0	0.3
97.5	2.0	0.5	89.6	10.0	0.5
97.3	2.0	0.7	89.4	9.9	0.7
97.0	2.0	1.0	89.1	9.9	1.0
96.6	2.0	1.5	88.7	9.9	1.5
96.1	2.0	2.0	88.2	9.8	2.0
95.1	1.9	2.9	87.4	9.7	2.9
93.3	1.9	4.8	85.7	9.5	4.8
91.6	1.9	6.5	84.1	9.3	6.5
89.1	1.8	9.1	81.8	9.1	9.1

Fe−Ti−M Ternary Oxides. For the Fe−Ti−M ternary oxides, we examined 25 kinds of M elements (Al, B, Ba, Bi, Ca, Ce, Co, Cr, Cu, Dy, In, La, Mg, Mn, Nb, Ni, Pb, Sb, Si, Sm, Sn, Sr, Ta, Y, and Zn). Using an M content range of 0−9.1 mol %, a set of 26 samples was created for each M, as listed in Table 1. Figure 2 shows the influence of the M elements on photocurrent. In the case of Fe−Ti ratio of 98:2 (Figure 2a), Ba, Ce, La, Sn, Sr, and Zn improved their

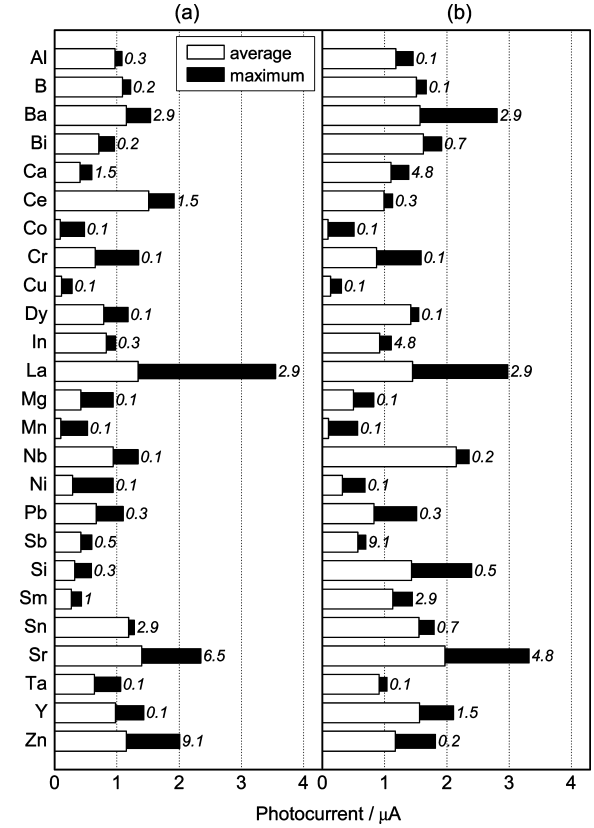

Figure 2. Photocurrents of Fe−Ti-M ternary oxides: Fe−Ti ratio of (a) 98:2 and (b) 90:10. The italicized values are the M atomic ratios at maximum photocurrents.

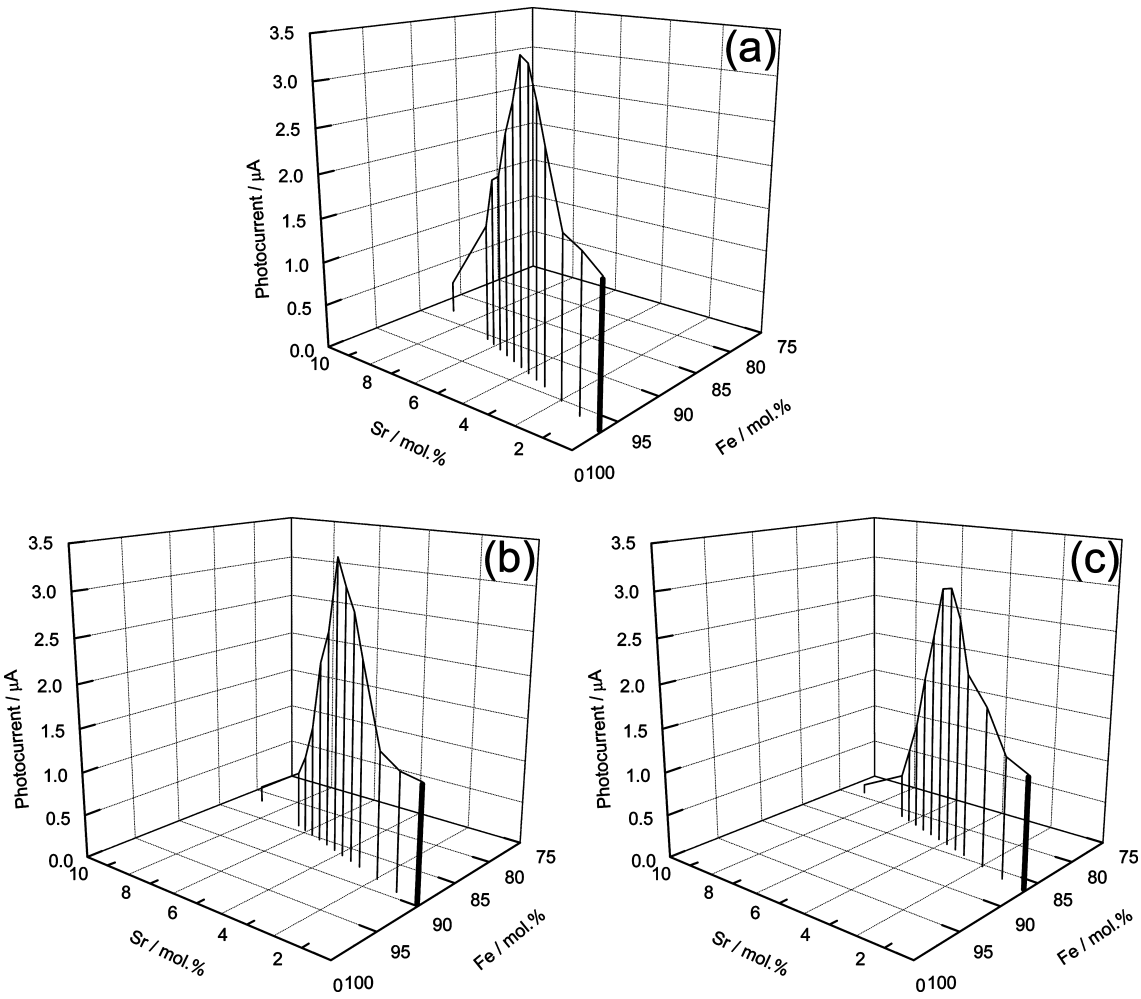

Figure 3. Dependence of the Sr ratio on the photocurrent in Fe−Ti−Sr ternary oxide photoelectrodes: Fe−Ti ratio of (a) 97:3, (b) 90:10, and (c) 87:13.

visible-light response, since their average photocurrents were higher than the 1.06 μA for Fe−Ti binary oxide in Figure 1. Adding La, Sr, and Zn also yielded high values of maximum photocurrent, over 2 μA. However, the addition of Ca, Co, Cu, Mn, Sb, Si, and Sm drastically decreased the visible-light response.

For the 90:10 Fe−Ti ratio in Figure 2b, the addition of B, Ba, Bi, La, Nb, Sn, Sr, and Y enhanced the average value of the photocurrent (1.36 μA in Figure 1). The samples containing Ba, La, Nb, Si, Sr, and Y showed high values of maximum photocurrent, over 2 μA. In contrast, adding Co, Cu, Mg, Mn, Ni, and Sb diminished the visible-light response of the oxides considerably. In general, ternary oxides based on the 90:10 Fe−Ti ratio exhibited higher photocurrent than those with a 98:2 ratio, in agreement with the binary oxide result of Figure 1.

Among the 25 elements tested, we find Sr to be the most effective, because it exhibited the highest maximum and average photocurrents for both Fe−Ti ratios. The photocurrent for the 90:10 system was more than 40% higher than for the 98:2 on for Sr addition. Cu was the least efficient additive among the 25 elements tested.

Consequently, we explored the effect of adding Sr on the Fe−Ti system at ratios near 90:10 in more detail. Figure 3 depicts the influence of Sr concentration on the photocurrent for the Fe−Ti ratio = 97:3, 90:10, and 87:13 systems. The photocurrent initially increased with the Sr ratio, reached a maximum at about 5 mol % of Sr, and then decreased drastically for all Fe−Ti ratios studied. Sr addition over 6 mol % adversely affected the visible-light response. Among the samples examined, the highest value of photocurrent, 3.34 μA, was obtained for $Fe_{86.1}Ti_{9.6}Sr_{4.3}O_x$, in agreement with the finding in Figure 2 that $Fe_{85.7}Ti_{9.5}Sr_{4.8}O_x$ exhibited the maximum photocurrent. This proves the reproducibility of our combinatorial search.

Oxide Characterization. To investigate the reason why the $Fe_{86.1}Ti_{9.6}Sr_{4.3}O_x$ (FeTiSrO) sample gave the highest photocurrent, several kinds of characterization were carried out. For comparison, Fe oxide (FeO), Fe−Ti binary oxide (FeTiO), and Fe−Sr binary oxide (FeSrO) with compositions corresponding to FeTiSrO and prepared by spin coating were also characterized. The photocurrent increased in the order: FeO < FeSrO < FeTiO < FeTiSrO, irrespective of the preparation method.

Figure 4 shows the SEM images of the different oxides. Porous structures were observed in all cases. FeO sample in Figure 4a comprised ~50 nm diameter grains. Grains ~60 nm in diameter were found in FeTiO (Figure 4b). However, some of the grains were rodlike, and the size distribution was larger than for FeO. The shapes of the grains for FeSrO

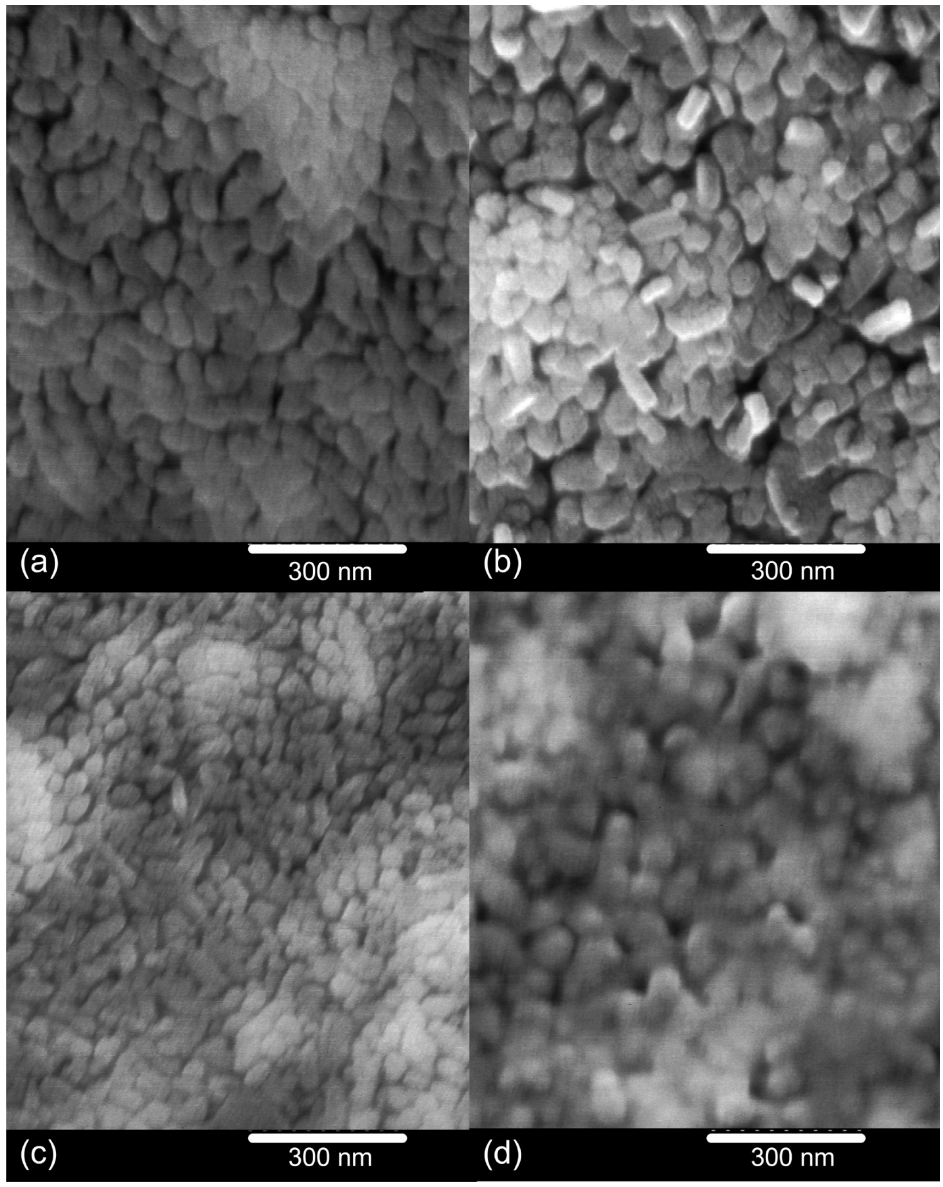

Figure 4. SEM images of semiconductor film surfaces: (a) FeO, (b) FeTiO, (c) FeSrO, and (d) FeTiSrO.

in Figure 4c were similar to those for FeO, but their sizes were smaller, approximately 30 nm. Unlike FeO, FeTiO, and FeSrO, the particles in FeTiSrO (Figure 4d) appeared fused and interconnected. They were approximately 70 nm in diameter.

Figure 5 shows the XRD spectra of the four oxides. Unlike in other characterizations, samples used for XRD were not film but powder, prepared by calcination of the precursor solution. The FeO sample in Figure 5a exhibited peaks that correspond to α-Fe_2O_3 (Hematite, JCPDS #33−0664, Figure 5e) at 24.2°, 33.2°, 35.6°, 40.9°, 49.5°, 54.1°, 62.4°, and 64.0°. At the same time, a tiny peak at 35.2° assigned to Fe_3O_4 (magnetite, JCPDS #19-0629) was discernible at the shoulder of an intense peak at 35.6°. The FeTiO sample in Figure 5b had peaks only due to α-Fe_2O_3, such as (104) and (110) reflections, suggesting Ti-doping of the hematite.[19]

Many peaks corresponding to $SrFe_{12}O_{19}$ (JCPDS #33-1340, Figure 5e) at 30.4°, 32.4°, 34.2°, 37.2°, 40.4°, 42.6°, 55.2°, 56.9°, and 63.2° appeared in the FeSrO sample (Figure 5c),

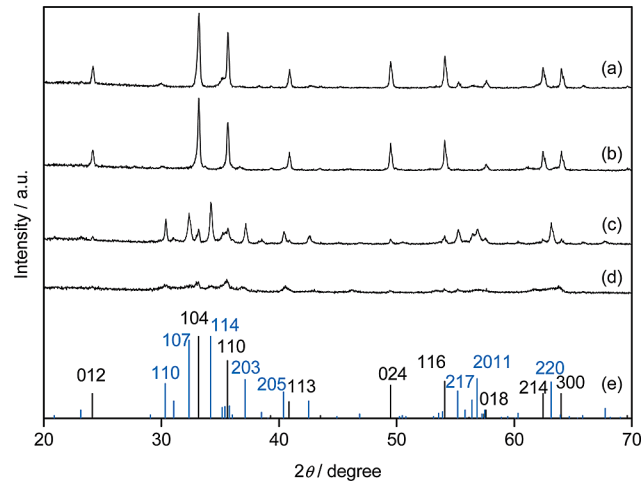

Figure 5. X-ray diffraction patterns of (a) FeO, (b) FeTiO, (c) FeSrO, (d) FeTiSrO, and (e) standard powder pattern of α-Fe_2O_3 (hematite: black lines with plane indices) and $SrFe_{12}O_{19}$ (blue lines with plane indices).

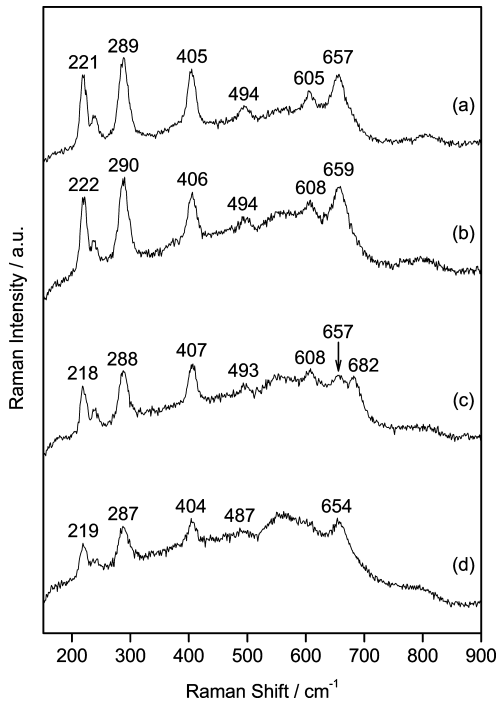

Figure 6. Raman spectra of semiconductor films: (a) FeO, (b) FeTiO, (c) FeSrO, and (d) FeTiSrO.

besides the weaker peaks due to α-Fe_2O_3 at 33.2°, 35.7°, 49.5°, and 54.1°, as well as Fe_3O_4 at 35.2°. Peaks corresponding to $SrFe_{12}O_{19}$ at 30.2° and 40.5° as well as α-Fe_2O_3 at 35.6° were also observed for the FeTiSrO sample in Figure 5d but were broader and weaker than those for the FeO, FeTiO, and FeSrO samples. These findings reveal that Sr as well as Ti is incorporated into the hematite for the FeTiSrO sample.

The crystalline sizes estimated from the XRD line broadening of the α-Fe_2O_3 (104) peak at $2\theta = 33.2°$ by the Scherrer equation are 36 nm for the FeO sample, 42 nm for the FeTiO one, and 24 nm for the FeSrO one. The crystalline size of the FeTiSrO sample could not be determined because the peak was very broad and weak; however, its trend among the three samples is consistent with the grain size observed by SEM in Figure 4.

The Raman spectra of the films are shown in Figure 6. The spectrum of FeO sample in Figure 6a is typical of an α-Fe_2O_3 phase showing peaks at 221, 289, 405, 494, and 605 cm^{-1}. These peaks matched well with the previously reported Raman data for hematite.[21–23] The band at 657 cm^{-1} may be due to either a magnetite[16,24] or the result of the breakdown in Raman symmetry selection rules induced by short-range order such as nanoscale dimensions or lattice defects.[16,21–23] Judging from the low intensity of the XRD spectrum in Figure 5a, this band would not be attributed to Fe_3O_4 but for defects. Five modes of α-Fe_2O_3 and one disorder-related mode were also found in FeTiO and FeSrO samples (Figure 6b,c). Besides, one $SrFe_{12}O_{19}$ mode appeared at 682 cm^{-1} for the FeSrO sample in Figure 6c,[25] in agreement with the XRD observation in Figure 5c. $SrFe_{12}O_{19}$ itself seems to have no visible-light responsiveness. The peak at around 610 cm^{-1} was not distinguished in the FeTiSrO sample (Figure 6d); however, it was also assigned to the hematite. In addition, there was a peak attributed to surface

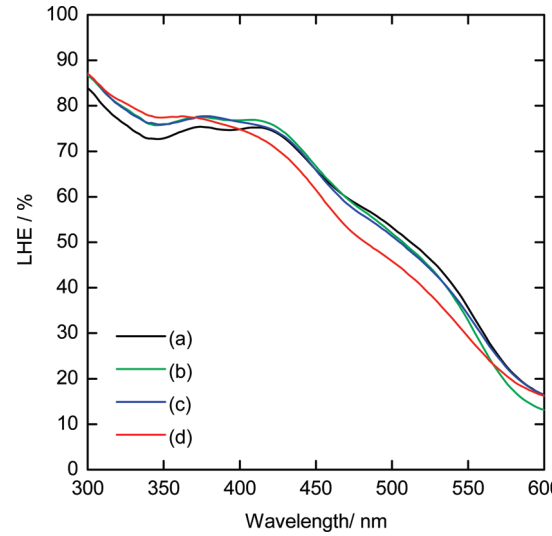

Figure 7. Light-harvesting efficiency (LHE) spectra of semiconductor films: (a) FeO, (b) FeTiO, (c) FeSrO, and (d) FeTiSrO.

and grain boundary disorder[22] detected at 654 cm^{-1} for all four samples.

Optical properties of the semiconductor films were studied by UV−vis spectroscopy. LHE spectra of the films are given in Figure 7. The LHE values for all samples were high, and over 80% of the values came from the short-wavelength region of the spectra. However, the values gradually decreased for longer wavelengths. As the wavelengths reached the characteristic optical absorption threshold for hematite (~600 nm),[23] the LHE dropped off rapidly. Little difference in LHE spectra was found among the four samples; that is, efficient visible-light absorption for α-Fe_2O_3 was preserved in Sr and Ti doping.

On the basis of the characterization results, we can explain why the $Fe_{86.1}Ti_{9.6}Sr_{4.3}O_x$ (FeTiSrO) sample exhibited the highest photocurrent as follows. Ti doping of α-Fe_2O_3 evidenced by XRD and Raman spectroscopy improved the short hole diffusion length in a hematite (2−4 nm,[26] 20 nm[27]). This is because the hole diffusion length in TiO_2 is 800 nm and is much longer than in α-Fe_2O_3.[28,29] Sr as well as Ti doping into hematite induces interconnection of nanocrystalline hematite particles, as demonstrated by SEM observations, leading to the minimization of the electron/hole transfer distances. The doping leaves high visible light absorbance unchanged,[29–31] as evaluated by UV−vis spectroscopy. As a result, recombination between photogenerated electrons and holes is suppressed in the FeTiSrO photoelectrode: more electrons and holes are forced to separate under an applied voltage. These are then detected as an increase in the photocurrent.

In the field of photocatalyst, the codoping method with two elements is often adopted to neutralize charge balance in the semiconductors. There is a possibility that Sr also maintains the charge balance in the crystal lattice of Fe_2O_3 by codoping with Ti. Kudo and co-workers studied the visible-light response of TiO_2 and $SrTiO_3$ codoped by Cr/Sb,[5] Rh/Sb,[32] Ni/Ta, and Ni/Nb.[33] They found that the photocatalytic activity of TiO_2 codoped with Cr/Sb, Rh/Sb, Ni/Ta, and Ni/Nb was much higher than that of TiO_2 doped

only with Cr, Rh, or Ni. The authors explained that the 5+ cations of Sb, Ta, and Nb codoped with the 3+ ones of Cr and Rh and the 2+ one of Ni maintain the charge balance of Ti^{4+}. This suppressed the formation of Cr^{6+}, Rh^{4+}, and Ni^{3+} ions or oxygen defects which serve as recombination centers. Hashimoto and co-workers also found that Ta/N codoping enhanced photocatalytic activities of N-doped TiO_2 thin films under visible light due to the charge compensation by Ta^{5+} as well as N^{3-} for Ti^{4+} and O^{2-}.[34] Dai and co-workers investigated the electronic and optical properties of N/La codoped $SrTiO_3$ by means of density functional calculations to explore the physical and chemical origin of its photocatalytic activity under visible light.[35] They demonstrated theoretically that no localized states serving as electron−hole recombination centers appeared within the N/La codoped $SrTiO_3$. On the basis of these findings, the codoped Sr^{2+} ions with Ti^{4+} should play a role in charge compensation for Fe^{3+} to prevent the formation of recombination centers between photogenerated electrons and holes, leading to enhanced visible-light response. As mentioned above, Ba addition to the Fe−Ti binary oxide also increased the photocurrent, supporting the theory for a dication. However, Mg and Ca were not effective in spite of dipositive ion. It may be due to the difference of doping condition into Fe_2O_3 lattice and/or the misalignment of doping amount for the charge compensation. Sr may also influence the electronic band structure of α-Fe_2O_3 although only Ti doping caused no change in it.[36]

La as well as Ba was also one of the most effective elements, but more detailed investigations of them will be reported in a forthcoming paper. The highest value of photocurrent, 3.55 μA, was obtained for $Fe_{95.1}Ti_{1.9}La_{2.9}O_x$, as shown in Figure 2a. Promotion effects of La doping have also been reported on the photocatalysts such as $NaTaO_3$,[37,38] TiO_2,[39] ZnO,[40] $Bi_4Ti_3O_{12}$,[41] and $AgNbO_3$.[42] Enhanced photocatalytic activity may be due to smaller particle size,[37,40,41] larger surface area,[40,42] ordered surface nanostep structure,[37] and inhibition on phase transformation[39] but is less well understood. Further works need to be investigated on the discovered Fe−Ti−La oxide.

Conclusion

We have successfully applied the high-throughput screening system to discover new ternary, visible-light responsive, n-type semiconductors, $Fe_{86.1}Ti_{9.6}Sr_{4.3}O_x$. The results of SEM, XRD, Raman, and UV−vis spectroscopy for the photoelectrode suggest that Sr as well as Ti suppress the recombination between photogenerated electrons and holes for high LHE α-Fe_2O_3. This leads to enhancement of visible-light responsiveness.

Acknowledgment. This study was supported by the New Energy and Industrial Technology Development Organization (NEDO) of Japan.

Supporting Information Available. Potential−current curves of samples. This material is available free of charge via the Internet at http://pubs.acs.org.

References and Notes

(1) Fujishima, A.; Honda, K. *Nature* **1972**, *238*, 37–38.
(2) Fujishima, A.; Hashimoto, K.; Watanabe, T. *TiO_2 Photocatalysis Fundamentals and Applications*; BKC: Tokyo, 1999.
(3) Zou, Z.; Ye, J.; Sayama, K.; Arakawa, H. *Nature* **2001**, *414*, 625–627.
(4) Domen, K.; Kondo, J. N.; Hara, M.; Takata, T. *Bull. Chem. Soc. Jpn.* **2000**, *73*, 1307–1331.
(5) Kato, H.; Kudo, A. *J. Phys. Chem. B* **2002**, *106*, 5029–5034.
(6) Kudo, A.; Ueda, K.; Kato, H.; Mikami, I. *Catal. Lett.* **1998**, *53*, 229–230.
(7) Jaramillo, T. F.; Ivanovskaya, A.; McFarland, E. W. *J. Comb. Chem.* **2002**, *4*, 17–22.
(8) Baeck, S.-H.; Jaramillo, T. F.; Brändli, C.; McFarland, E. W. *J. Comb. Chem.* **2002**, *4*, 563–568.
(9) Jaramillo, T. F.; Baeck, S.-H.; Kleiman-Shwarsctein, A.; Choi, K. S.; Stucky, G. D.; McFarland, E. W. *J. Comb. Chem.* **2005**, *7*, 264–271.
(10) Woodhouse, M.; Herman, G. S.; Parkinson, B. A. *Chem. Mater.* **2005**, *17*, 4318–4324.
(11) Woodhouse, M.; Parkinson, B. A. *Chem. Mater.* **2008**, *20*, 2495–2502.
(12) Katz, J. E.; Gingrich, T. R.; Santori, E. A.; Lewis, N. S. *Energy Environ. Sci.* **2009**, *2*, 103–112.
(13) Santato, C.; Ulmann, M.; Augustynski, J. *J. Phys. Chem. B* **2001**, *105*, 936–940.
(14) Sayama, K.; Nomura, A.; Zou, Z.; Abe, R.; Abe, Y.; Arakawa, H. *Chem. Commun.* **2003**, 2908–2909.
(15) Aroutiounian, V. M.; Arakelyan, V. M.; Shahnazaryan, G. E. *Sol. Energy* **2005**, *78*, 581–592.
(16) Sartoretti, C. J.; Alexander, B. D.; Solarska, R.; Rutkowska, I. A.; Augustynski, J. *J. Phys. Chem. B* **2005**, *109*, 13685–13692.
(17) Solarska, R.; Alexander, B. D.; Augustynski, J. *C. R. Chim.* **2006**, *9*, 301–306.
(18) Miyake, H.; Kozuka, H. *J. Phys. Chem. B* **2005**, *109*, 17951–17956.
(19) Arai, T.; Konishi, Y.; Iwasaki, Y.; Sugihara, H.; Sayama, K. *J. Comb. Chem.* **2007**, *9*, 574–581.
(20) Arai, T.; Yanagida, M.; Konishi, Y.; Iwasaki, Y.; Sugihara, H.; Sayama, K. *AIP Conf. Proc.* **2008**, *987*, 26–29.
(21) Glasscock, J. A.; Barnes, P. R. F.; Plumb, I. C.; Bendavid, A.; Martin, P. J. *Thin Solid Films* **2008**, *516*, 1716–1724.
(22) Tahir, A. A.; Wijayantha, K. G. U.; Saremi-Yarahmadi, S.; Mazhar, M.; McKee, V. *Chem. Matter.* **2009**, *21*, 3763–3772.
(23) Saremi-Yarahmadi, S.; Wijayantha, K. G. U.; Tahir, A. A.; Vaidhyanathan, B. *J. Phys. Chem. C* **2009**, *113*, 4768–4778.
(24) Duret, A.; Grätzel, M. *J. Phys. Chem. B* **2005**, *109*, 17184–17191.
(25) Zhang, L.; Li, Z. *J. Alloys Compd.* **2009**, *469*, 422–426.
(26) Kennedy, J. H.; Frese, K. W. *J. Electrochem. Soc.* **1978**, *125*, 709–714.
(27) Dare-Edwards, M. P.; Goodenough, J. B.; Hamnet, A.; Trevellick, P. R. *J. Chem. Soc. Faraday Trans. 1* **1983**, *79*, 2027–2041.
(28) Soedergren, S.; Hagfeldt, A.; Olsson, J.; Lindquist, S. E. *J. Phys. Chem.* **1994**, *98*, 5552–5556.
(29) Kay, A.; Cesar, I.; Grätzel, M. *J. Am. Chem. Soc.* **2006**, *128*, 15714–15721.
(30) Hodes, G.; Howell, I. D. J.; Peter, L. M. *J. Electrochem. Soc.* **1992**, *139*, 3136–3140.
(31) Hagfeldt, A.; Grätzel, M. *Chem. Rev.* **1995**, *95*, 49–68.
(32) Niishiro, R.; Konta, R.; Kato, H.; Chun, W.-J.; Asakura, K.; Kudo, A. *J. Phys. Chem. C* **2007**, *111*, 17420–17426.
(33) Niishiro, R.; Kato, H.; Kudo A., *Phys. Chem. Chem. Phys.* **2005**, *7*, 2241–2245.
(34) Obata, K.; Irie, H.; Hashimoto, K. *Chem. Phys.* **2007**, *339*, 1–192.

(35) Wei, W.; Dai, Y.; Guo, M.; Yu, L.; Huang, B. *J. Phys. Chem. C* **2009**, *113*, 15046–15050.
(36) Thimsen, E.; Biswas, S.; Lo, C. S.; Biswas, P. *J. Phys. Chem. C* **2009**, *113*, 2014–2021.
(37) Kato, H.; Asakura, K.; Kudo, A. *J. Am. Chem. Soc.* **2003**, *125*, 3082–3089.
(38) Matsumoto, Y.; Unal, U.; Tanaka, N.; Kudo, A.; Kato, H. *J. Solid State Chem.* **2004**, *177*, 4205–4212.
(39) Liqiang, J.; Xiaojun, S.; Baifu, X.; Baiqi, W.; Weimin, C.; Honggang, F. *J. Solid State Chem.* **2004**, *177*, 3375–3382.
(40) Anandan, S.; Vinu, A.; Lovely, K. L. P. S.; Gokulakrishnan, N.; Srinivasu, P.; Mori, T.; Murugesan, V.; Sivamurugan, V.; Ariga, K. *J. Mol. Catal. A: Chem.* **2007**, *266*, 149–157.
(41) Zhang, H.; Lü, M.; Liu, S.; Wang, L.; Xiu, Z.; Zhou, Y.; Qiu, Z.; Zhang, A.; Ma, Q. *Mater. Chem. Phys.* **2009**, *114*, 716–721.
(42) Li, G.; Kako, T.; Wang, D.; Zou, Z.; Ye, J. *Dalton Trans.* **2009**, 2423–2427.

CC9001845